Modeling of Cohesive Cracks in the Element-Free Galerkin Method

Preecha Soparat[1] and Pruettha Nanakorn[2]
Sirindhorn International Institute of Technology, Thammasat University
PO Box 22, Thammasat-Rangsit Post Office
Pathumthani 12121, Thailand
Tel: 0-2986-9009 Ext. 1906, Fax: 0-2986-9009 Ext. 1900
E-mail: [1]preecha@siit.tu.ac.th , [2]nanakorn@siit.tu.ac.th

Abstract

This study presents modeling of cohesive cracks in the Element-Free Galerkin (EFG) method. A cohesive crack is represented by several end-connected straight-line interface elements on which a constitutive law of cohesive cracks is directly applied. The stiffness equation is straightforwardly derived by including a term related to the energy dissipation along the interface elements in the weak form of the system equation. Using the interface elements in the EFG method allows cracks to propagate virtually without any constraint on their directions. Numerical results obtained from the proposed method for some benchmark tests of plain concrete beams are presented and compared with existing numerical and experimental results.

1. Introduction

In modeling crack propagation in quasi-brittle materials such as concrete, it is necessary to take into account the presence and the effect of a large nonlinear fracture process zone ahead of a crack tip. In the fracture process zone, various microevents, such as microcracking, crack deflection, crack branching, and crack bridging, occur and energy is dissipated. The fracture process zone has been found to be best represented as an extension of the actual crack that is subjected to a closing pressure as in the fictitious crack model [1]. The general form of the fictitious crack model allows both tensile and shear stresses to be transmitted across the surfaces of the crack. The magnitudes of these transmitted stresses are generally assumed to be functions of crack displacements.

Using the fictitious crack model in conjunction with the finite element method (FEM) to model cohesive crack propagation in two-dimensional problems has been receiving significant attention from many researchers [2-5]. However, FEM possesses intrinsic disadvantages when it is used in crack propagation problems. The most serious one is the representation of cracks in finite element (FE) models. The use of elements in FEM creates difficulties in the treatment of cracks that do not coincide with the FE mesh lines. Various numerical techniques have been developed to solve this crack representation problem in FEM. One of the well accepted techniques is to remesh the domain of the problem in each step of the crack evolution in such a way that the mesh lines remain coincident with the cracks throughout the evolution of the problem [2,4,6]. Several complex and robust mesh refinement algorithms have been developed [4,6]. These algorithms can be computationally more expensive than the assembly and solution processes. Another popular technique is to embed cracks directly into elements and modify the stiffnesses of the elements to incorporate the existence of the cracks within the elements [7,8,9]. However, with this technique, it is difficult to maintain the continuity of the crack line. As a result, the continuity of the crack line is mostly neglected. In addition, a spurious mode can also occur if the position and orientation of a crack are freely allowed within the element.

Recently, Belytschko et al. [10] proposed a new method called the Element-Free Galerkin (EFG) method for solving mechanical problems with arbitrary geometry. The EFG shape functions and their derivatives are constructed by using the moving least-square (MLS) approximation defined by Lancaster

RECEIVED 11 July, 2005
ACCEPTED 11 October, 2006

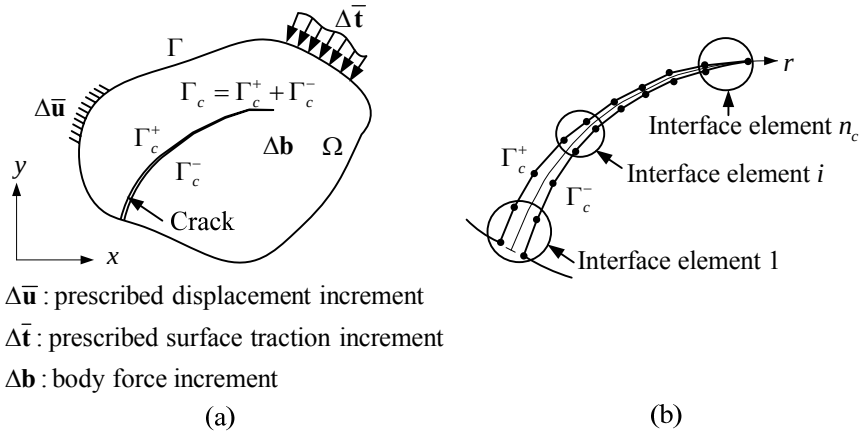

$\Delta\bar{\mathbf{u}}$: prescribed displacement increment

$\Delta\bar{\mathbf{t}}$: prescribed surface traction increment

$\Delta\mathbf{b}$: body force increment

(a) (b)

Fig. 1 Crack modeling by interface elements

and Salkauskas [11]. From a modeling viewpoint, the essential feature of the EFG method is that only nodal data and boundary descriptions are required to formulate the discrete Galerkin equations. A background-cell structure, which is independent of nodal points, is used for the procedure to compute the integral expression. Since the method requires no element, it is an excellent choice for solving crack propagation problems. Several extensions of the EFG method to model crack propagation have been proposed [12-15]. However, all of these works are related to brittle cracks with no traction force between crack surfaces. The EFG method has been used to simulate dynamic crack growth in concrete by Belytschko et al. [16]. In their proposed method, cohesive cracks are not directly included in the weak form of the system equation. Instead, to simulate the effect of crack cohesion, the transmitted tensile stress across the crack surfaces is computed from the current crack opening displacement and is directly applied to the crack surfaces in the subsequent step of the calculation.

In this paper, a new way to model cohesive cracks in the EFG method for 2D domains is proposed. A cohesive curved crack is model by using straight-line interface elements connected to form the crack. These interface elements permit the constitutive law of cohesive cracks to be considered efficiently. In this study, the analysis is performed incrementally. To allow accurate results to be obtained without the need of iteration, the stiffness equation of the domain is constructed by directly including a term related to the energy dissipation along the interface elements in the weak form of the global system equation. The validity and efficiency of the proposed method are shown by solving several numerical problems. The obtained results are compared with results by FEM and experiments reported in the literature.

2. Modeling of Cohesive Cracks in the Element-Free Galerkin Method

Consider a two-dimensional domain Ω in the xy plane with boundary Γ in Fig. 1(a). The boundary Γ is subdivided into two parts, i.e., Γ_u where the displacement is prescribed, and Γ_t where the surface traction is prescribed. Assume further that there is a crack in the domain and it is represented as an additional boundary Γ_c inside Ω. The crack boundary Γ_c is composed of two opposite surfaces, i.e., Γ_c^+ and Γ_c^-, as shown in Fig. 1(a). In this study, the crack is modeled by using connected straight-line interface elements as shown in Fig. 1(b). Each interface element contains the two surfaces of the crack. Fig. 2(a) shows the i^{th} interface element and its local coordinate system whose origin is at the center of the element. The interface element has two coincident surfaces each of which has nodes at

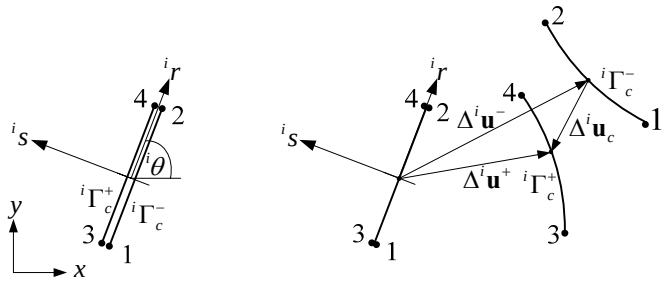

Fig. 2 Details of the interface element

its ends. The two surfaces are designated as the positive surface ${}^{i}\Gamma_c^+$ and the negative surface ${}^{i}\Gamma_c^-$. When the crack opens, the two surfaces move away from each other. The crack displacement increment $\Delta^i\mathbf{u}_c$ along the length of the element in the global coordinate system shown in Fig. 2(b) is expressed as

$$\Delta^i\mathbf{u}_c({}^ir) = \begin{Bmatrix}\Delta^i u_c \\ \Delta^i v_c\end{Bmatrix} = \Delta^i\mathbf{u}^+({}^ir) - \Delta^i\mathbf{u}^-({}^ir), \qquad (1)$$

where $\Delta^i\mathbf{u}^+$ and $\Delta^i\mathbf{u}^-$ are the displacement increments along the positive and negative surfaces of the element, respectively. These two displacement increments $\Delta^i\mathbf{u}^+$ and $\Delta^i\mathbf{u}^-$ are expressed in terms of the nodal displacement increment $\Delta\mathbf{U}$ as

$$\Delta^i\mathbf{u}^+({}^ir) = \mathbf{N}[{}^i\mathbf{x}^+({}^ir)]\Delta\mathbf{U}, \qquad (2)$$

$$\Delta^i\mathbf{u}^-({}^ir) = \mathbf{N}[{}^i\mathbf{x}^-({}^ir)]\Delta\mathbf{U}, \qquad (3)$$

where

$$\mathbf{N}(\mathbf{x}) = \begin{bmatrix} N_1(\mathbf{x}) & 0 & \dots & N_M(\mathbf{x}) & 0 \\ 0 & N_1(\mathbf{x}) & \dots & 0 & N_M(\mathbf{x}) \end{bmatrix}, \qquad (4)$$

$$\Delta\mathbf{U} = \begin{bmatrix}\Delta u_1 & \Delta v_1 & \dots & \Delta u_M & \Delta v_M\end{bmatrix}^{\mathrm{T}}. \qquad (5)$$

Here, ${}^i\mathbf{x}^+$ and ${}^i\mathbf{x}^-$ represent two opposite points at position ${}^ir$ on the positive and negative surfaces of the interface element, respectively. The subscript I in $N_I(\mathbf{x})$, Δu_I and Δv_I represent the node number while M represents the total number of nodes in the domain. In this study, the shape function matrix $\mathbf{N}(\mathbf{x})$ for the EFG method using the Gaussian weight function [14] is used. Nevertheless, during the construction of the shape function matrices, $\mathbf{N}[{}^i\mathbf{x}^+({}^ir)]$ and $\mathbf{N}[{}^i\mathbf{x}^-({}^ir)]$, the domains of influence of nodes are considered based on the visibility criterion [14]. The visibility criterion is necessary for constructing shape functions near a crack that contain the discontinuities in the displacement increments. The concept of this criterion is that the domain boundaries and any lines of cracks are treated as opaque objects during the construction of weight functions. Consider, in Fig. 3(a), node I that has a crack line within its domain of influence. The radius d_{mI}, which is used to determine the domain of influence of node I, is treated as a ray of light. When the ray encounters the opaque crack line, it is terminated and the area that is not reached by the ray is excluded from the domain of influence of node I. As a result, in Fig. 3(a), the shaded region becomes the modified domain of influence of node I. In consequence of the visibility criterion, nodes that are used in the approximation of $\Delta^i\mathbf{u}^+({}^ir)$ and $\Delta^i\mathbf{u}^-({}^ir)$ will be different as schematically shown in Fig. 3(b). This difference can be seen in the difference between $\mathbf{N}[{}^i\mathbf{x}^+({}^ir)]$ and $\mathbf{N}[{}^i\mathbf{x}^-({}^ir)]$.

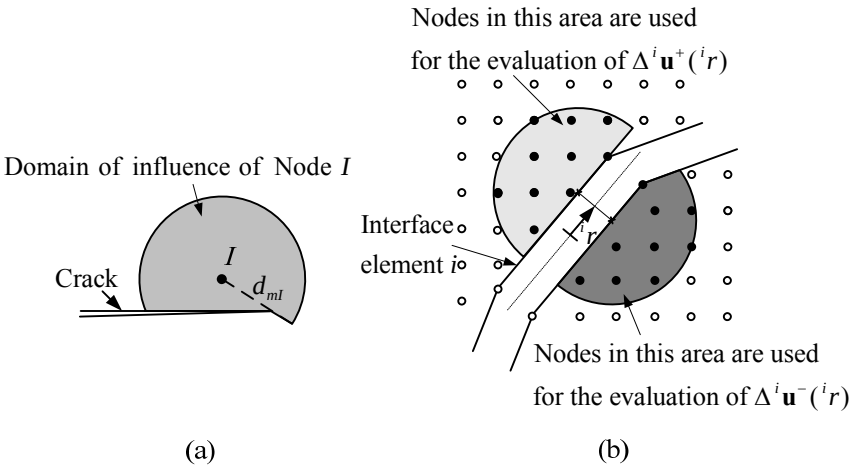

Fig. 3 Domain of influence near a crack

By substituting (2) and (3) into (1), the crack displacement increment $\Delta^i\mathbf{u}_c$ can be written as

$$\begin{aligned}\Delta^i\mathbf{u}_c({}^ir) &= \left(\mathbf{N}[{}^i\mathbf{x}^+({}^ir)]-\mathbf{N}[{}^i\mathbf{x}^-({}^ir)]\right)\Delta\mathbf{U} \\ &= {}^i\mathbf{N}_c({}^ir)\Delta\mathbf{U},\end{aligned} \tag{6}$$

where ${}^i\mathbf{N}_c({}^ir)$ is the crack shape function matrix defined as

$${}^i\mathbf{N}_c({}^ir) = \mathbf{N}[{}^i\mathbf{x}^+({}^ir)] \; - \; \mathbf{N}[{}^i\mathbf{x}^-({}^ir)]\,. \tag{7}$$

Constitutive laws for cohesive cracks are normally described based on local coordinate systems of the cracks. Therefore, the crack displacement increment in the local ${}^ir-{}^is$ coordinate system $\Delta^i\hat{\mathbf{u}}_c$ must be introduced, i.e.,

$$\Delta^i\hat{\mathbf{u}}_c({}^ir) = \begin{Bmatrix}\Delta^i\hat{u}_c({}^ir)\\ \Delta^i\hat{v}_c({}^ir)\end{Bmatrix} = {}^i\hat{\mathbf{T}}\Delta^i\mathbf{u}_c({}^ir)\,, \tag{8}$$

where $\Delta^i\hat{u}_c$ and $\Delta^i\hat{v}_c$ represent the crack sliding and opening displacement increments, respectively. In addition, ${}^i\hat{\mathbf{T}}$ is the transformation matrix defined as

$${}^i\hat{\mathbf{T}} = \begin{bmatrix}\cos({}^i\theta) & \sin({}^i\theta)\\ -\sin({}^i\theta) & \cos({}^i\theta)\end{bmatrix}. \tag{9}$$

Here, ${}^i\theta$ is the angle between the local ${}^ir$ axis and the global x axis as shown in Fig. 2(a).

Write the transmitted crack traction increment $\Delta^i\hat{\mathbf{t}}_c$ in the local coordinate system as

$$\Delta^i\hat{\mathbf{t}}_c = \begin{Bmatrix}\Delta^i\hat{t}_r\\ \Delta^i\hat{t}_s\end{Bmatrix}. \tag{10}$$

Here, $\Delta^i\hat{\mathbf{t}}_c$ is defined as the traction increment exerted by the positive surface to the negative surface of the interface element.

Next, the crack constitutive law is introduced as

$$\Delta^i\hat{\mathbf{t}}_c({}^ir) = \hat{\mathbf{D}}_c\Delta^i\hat{\mathbf{u}}_c({}^ir)\,, \tag{11}$$

where $\hat{\mathbf{D}}_c$ is the crack constitutive matrix defined as

$$\hat{\mathbf{D}}_c = \begin{bmatrix}D^{II} & 0\\ 0 & D^I\end{bmatrix}, \tag{12}$$

where D^I and D^{II} represent the mode I and mode II crack modulus, respectively. Note that

D^I and D^{II} are functions of the crack opening and sliding displacements.

By employing (6), (8) and (11), the local crack displacement increment $\Delta^i\hat{\mathbf{u}}_c$ and local crack traction increment $\Delta^i\hat{\mathbf{t}}_c$ are written in terms of the nodal displacement increment $\Delta\mathbf{U}$ as

$$\Delta^i\hat{\mathbf{u}}_c({}^ir) = {}^i\hat{\mathbf{T}}\,{}^i\mathbf{N}_c({}^ir)\Delta\mathbf{U}, \tag{13}$$

$$\Delta^i\hat{\mathbf{t}}_c({}^ir) = \hat{\mathbf{D}}_c\,{}^i\hat{\mathbf{T}}\,{}^i\mathbf{N}_c({}^ir)\Delta\mathbf{U}. \tag{14}$$

In this study, to simulate crack growth, the existing crack is lengthened, in each incremental step, by extending the crack line using a new interface element. The extension of the crack is assumed to be of mode I. Therefore, the extension occurs when the maximum principal tensile stress ahead of the crack tip reaches the value of the tensile strength of the material. The direction of the extension is naturally perpendicular to the direction of this maximum principal tensile stress.

3. Derivation of the Stiffness Matrix Equation

The weak form of the problem can be written as

$$\begin{bmatrix} \int_\Omega \delta(\Delta\boldsymbol{\varepsilon}^{\mathrm{T}})\Delta\boldsymbol{\sigma}d\Omega \\ -\int_\Omega \delta(\Delta\mathbf{u}^{\mathrm{T}})\Delta\mathbf{b}d\Omega - \int_{\Gamma_t} \delta(\Delta\mathbf{u}^{\mathrm{T}})\Delta\bar{\mathbf{t}}d\Gamma \\ -\int_{\Gamma_u} \delta(\Delta\boldsymbol{\lambda}^{\mathrm{T}})\left(\Delta\mathbf{u} - \Delta\bar{\mathbf{u}}\right)d\Gamma \\ -\int_{\Gamma_u} \delta(\Delta\mathbf{u}^{\mathrm{T}})\Delta\boldsymbol{\lambda}d\Gamma \end{bmatrix} + \left[\sum_{i=1}^{n_c}\int_{{}^i\Gamma_c^-} \delta(\Delta^i\hat{\mathbf{u}}_c^{\mathrm{T}})\Delta^i\hat{\mathbf{t}}_c d\Gamma\right] = 0. \tag{15}$$

The above weak form consists of two parts. The terms in the first brackets are the well-known terms found in the weak form for the EFG method which requires the use of Lagrange multipliers to enforce the essential boundary conditions [10]. Here, $\Delta\boldsymbol{\lambda}$ denotes a vector containing Lagrange multiplier increments defined as

$$\Delta\boldsymbol{\lambda} = \begin{Bmatrix} \Delta\lambda_x \\ \Delta\lambda_y \end{Bmatrix}. \tag{16}$$

The term in the second brackets is associated to the energy dissipation from the cohesive crack which is modeled by n_c interface elements. The other symbols are either mentioned earlier or self-evident.

In this study, the constitutive law of the material in the analysis is assumed to be linear elastic, i.e.,

$$\Delta\boldsymbol{\sigma} = \mathbf{D}\Delta\boldsymbol{\varepsilon}, \tag{17}$$

where $\mathbf{D}$ is the constitutive matrix. By employing the EFG shape functions with the Gaussian weight function [14], the displacement increment vector $\Delta\mathbf{u}$ and the strain increment vector $\Delta\boldsymbol{\varepsilon}$ are written in terms of the nodal displacement increment vector $\Delta\mathbf{U}$ as

$$\Delta\mathbf{u} = \mathbf{N}\Delta\mathbf{U}, \tag{18}$$

$$\Delta\boldsymbol{\varepsilon} = \mathbf{B}\Delta\mathbf{U}, \tag{19}$$

where $\mathbf{N}$ and $\mathbf{B}$ represent the shape function matrix and its derivative matrix, respectively. Note that $\mathbf{N}$ must be constructed by using the domains of influence of nodes that are based on the visibility criterion [14].

The Lagrange multiplier increment $\Delta\boldsymbol{\lambda}$ is interpolated from its nodal values by using Lagrange interpolation as

$$\Delta\boldsymbol{\lambda}(\mathbf{x}) = \mathbf{N}_\lambda(r_u)\Delta\boldsymbol{\Lambda} \qquad \mathbf{x}\in\Gamma_u, \tag{20}$$

where $\mathbf{N}_\lambda(r_u)$ is a Lagrange-interpolant matrix and r_u denotes the arc length along the boundary Γ_u. In addition, $\Delta\boldsymbol{\Lambda}$ is a vector

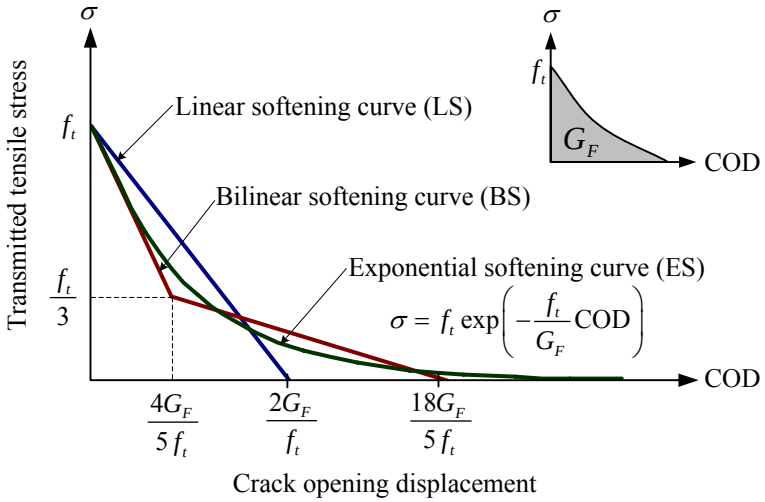

Fig. 4 Tension-softening curves

containing nodal Lagrange multiplier increments of all the nodes on the boundary Γ_u.

By substituting (13)-(14) and (17)-(20) into (15), the weak form becomes

$$\begin{bmatrix} \delta\left(\Delta\mathbf{U}^{\mathrm{T}}\right)\int_{\Omega}\mathbf{B}^{\mathrm{T}}\mathbf{D}\mathbf{B}d\Omega\Delta\mathbf{U} - \delta\left(\Delta\mathbf{U}^{\mathrm{T}}\right)\int_{\Omega}\mathbf{N}^{\mathrm{T}}\Delta\mathbf{b}d\Omega \\ -\delta\left(\Delta\mathbf{U}^{\mathrm{T}}\right)\int_{\Gamma_t}\mathbf{N}^{\mathrm{T}}\Delta\bar{\mathbf{t}}d\Gamma - \delta\left(\Delta\boldsymbol{\Lambda}^{\mathrm{T}}\right)\int_{\Gamma_u}\mathbf{N}_{\lambda}^{\mathrm{T}}\mathbf{N}d\Gamma\Delta\mathbf{U} \\ +\delta\left(\Delta\boldsymbol{\Lambda}^{\mathrm{T}}\right)\int_{\Gamma_u}\mathbf{N}_{\lambda}^{\mathrm{T}}\Delta\bar{\mathbf{u}}d\Gamma - \delta\left(\Delta\mathbf{U}^{\mathrm{T}}\right)\int_{\Gamma_u}\mathbf{N}^{\mathrm{T}}\mathbf{N}_{\lambda}d\Gamma\Delta\boldsymbol{\Lambda} \end{bmatrix} + \left[\delta\left(\Delta\mathbf{U}^{\mathrm{T}}\right)\sum_{i=1}^{n_c}\int_{{}^{i}\Gamma_c^-}{}^{i}\mathbf{N}_c^{\mathrm{T}}\,{}^{i}\hat{\mathbf{T}}^{\mathrm{T}}\hat{\mathbf{D}}_c\,{}^{i}\hat{\mathbf{T}}\,{}^{i}\mathbf{N}_c d\Gamma\Delta\mathbf{U}\right] = 0. \tag{21}$$

Finally, since $\delta\left(\Delta\mathbf{U}^{\mathrm{T}}\right)$ and $\delta\left(\Delta\boldsymbol{\Lambda}^{\mathrm{T}}\right)$ are arbitrary, the stiffness equation is written as

$$\begin{bmatrix} \mathbf{K} & \mathbf{G} \\ \mathbf{G}^{T} & 0 \end{bmatrix}\begin{Bmatrix} \Delta\mathbf{U} \\ \Delta\boldsymbol{\Lambda} \end{Bmatrix} = \begin{Bmatrix} \Delta\mathbf{R}_1 \\ \Delta\mathbf{R}_2 \end{Bmatrix}, \tag{22}$$

where

$$\mathbf{K} = \int_{\Omega}\mathbf{B}^{\mathrm{T}}\mathbf{D}\mathbf{B}d\Omega + \sum_{i=1}^{n_c}\int_{{}^{i}\Gamma_c^-}{}^{i}\mathbf{N}_c^{\mathrm{T}}\,{}^{i}\hat{\mathbf{T}}^{\mathrm{T}}\hat{\mathbf{D}}_c\,{}^{i}\hat{\mathbf{T}}\,{}^{i}\mathbf{N}_c d\Gamma, \tag{23}$$

$$\mathbf{G} = -\int_{\Gamma_u}\mathbf{N}^{\mathrm{T}}\mathbf{N}_{\lambda}d\Gamma, \tag{24}$$

$$\Delta\mathbf{R}_1 = \int_{\Omega}\mathbf{N}^{\mathrm{T}}\Delta\mathbf{b}d\Omega + \int_{\Gamma_t}\mathbf{N}^{\mathrm{T}}\Delta\bar{\mathbf{t}}d\Gamma, \tag{25}$$

$$\Delta\mathbf{R}_2 = -\int_{\Gamma_u}\mathbf{N}_{\lambda}^{\mathrm{T}}\Delta\bar{\mathbf{u}}d\Gamma. \tag{26}$$

4. Results

The validity and efficiency of the proposed method are shown by solving three numerical problems. They are the three-point bending test, the four-point single-notched shear test, and the four-point double-notched shear test, all of plain concrete. The shear fracture resistance is neglected in this study. However, a very small numerical value is used for the mode II crack modulus D^{II} in order to prevent spurious instability. The three tests are analyzed with three different types of tension softening curve, i.e., the linear softening curve [2], bilinear softening curve [3], and exponential softening curve [4]. The three tension softening curves are shown in Fig. 4. The details of the material properties used in all problems are shown in Table 1.

4.1 Three-Point Bending Test

The most commonly used configuration to investigate the mode I crack propagation in plain concrete is a notched beam subjected to three-point bending. In this study, the beam

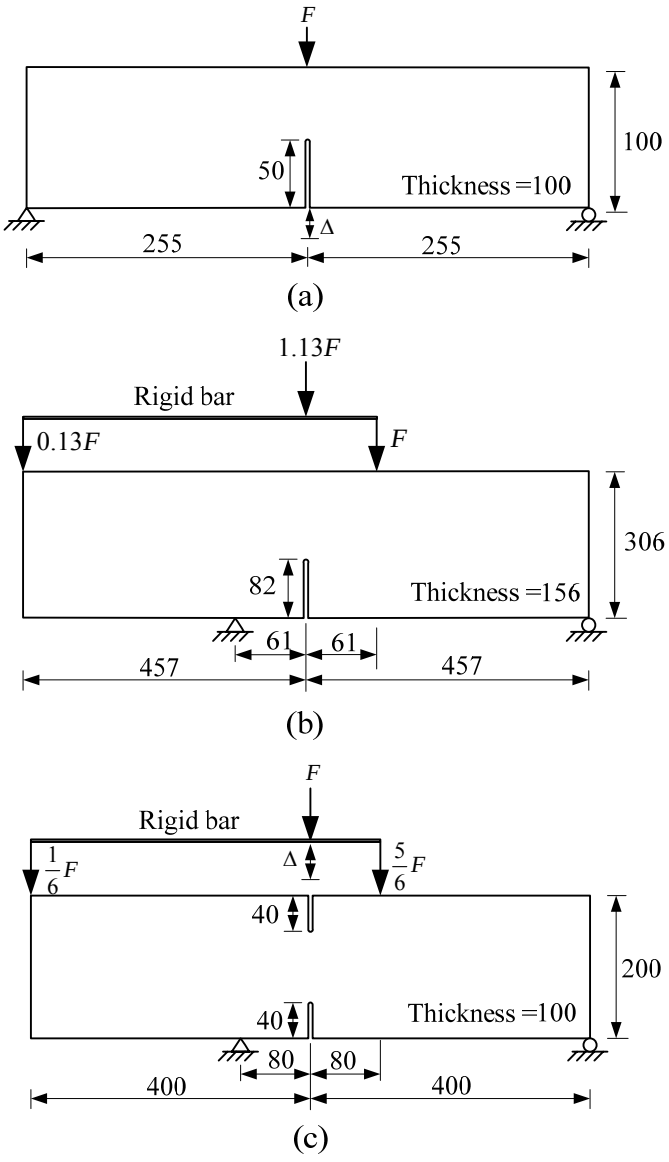

Fig. 5 Geometry of the numerical examples (unit: mm)

shown in Fig. 5(a) is used. The depth, length and thickness of the beam are 100 mm, 510 mm, and 100 mm, respectively. The ratio between the notched depth and the beam depth is equal to 0.5. The crack mount opening displacement (CMOD) is used as a controlling parameter of loading.

The obtained results are compared with a result from FE analysis by Prasad and Krishnamoorthy [4] and experimental results by Körmeling and Reinhardt [17] as shown in Fig. 6(a). It is found that the obtained responses are in good agreement with the FE and experimental results. However, the results obtained with the bilinear and exponential tension-softening curves agree better with the experimental results. The result obtained with the linear tension-softening curve agrees closely with the result by Prasad and Krishnamoorthy [4] which is also obtained with the linear tension-softening curve. The bilinear and exponential tension-softening curves have steeper initial slopes than that of the linear curve. A steeper initial slope means that the material is initially more brittle. As a result, the results obtained with the bilinear and exponential tension-softening curves are expected to have lower peak loads than those

obtained with the linear tension-softening curve.

4.2 Four-Point Single-Notched Shear Test

The second numerical example is the four-point single-notched shear test. In this study, the beam shown in Fig. 5(b) is employed. The depth, length and thickness of the beam are 306 mm, 914 mm and 156 mm, respectively. In this problem, the crack mount sliding displacement (CMSD) is used as a controlling parameter of loading.

The obtained results are compared with a result from FE analysis by Alfaiate et al. [3] and experimental results by Arrea [18] as shown in Fig. 6(b). Note that Alfaiate et al. [3] use the bilinear tension-softening curve in their analysis. It is found from the comparison that the obtained responses are generally in good agreement with the FE results by Alfaiate et al. [3]. Nevertheless, the obtained numerical results are found to significantly have lower peak loads than those of the experimental results. In fact, it can be observed that the initial slopes of the load-CMSD curves from the obtained numerical results and the experimental results are quite different. Since the initial slope depends on the elastic stiffness of the beam, the differences in the initial slopes imply that the Young's modulus used in the numerical computations may not really be accurate. The obtained crack paths are also compared with the FE result by Alfaiate et al. [3] and the experimental results by Arrea [18] in Fig. 7(a). It can be seen that all crack paths obtained by the numerical computations agree very well. However, they are slightly different from the experimental results.

4.3 Four-Point Double-Notched Shear Test

The last numerical example is the four-point double-notched shear test. The geometry of the tested beam and the boundary conditions are shown in Fig. 5(c). The depth, length, and thickness of the beam are 200 mm, 800 mm, and 100 mm, respectively. The crack mount sliding displacement (CMSD) is used as a controlling parameter of loading.

The obtained results are compared with FE and experimental results by Bocca et al. [2] in Fig. 6(c). In general, good agreements between the obtained results and the FE and experimental results can be observed. The obtained results with the bilinear and exponential softening curves seem to agree better with the experimental result. The FE result by Bocca et al. [2] which is obtained with the linear tension-softening curve is found to have a higher peak load than those of the experimental result and the proposed result with the same type of the tension softening curve. Nevertheless, its postpeak response agrees well with the experimental result as well as the proposed results obtained with the bilinear and exponential tension-softening curves. In Fig. 7(b), the crack paths are presented. All of the crack paths agree very well.

Table 1 Material properties

Problem	E (GPa)	ν	f_t (MPa)	G_F (N/m)	Softening Curve
Three-point bending test	20.0	0.20	2.40	113.0	Linear (LS)
					Bilinear (BS)
					Exponential (ES)
Four-point single-notched shear test	24.8	0.18	2.80	100.0	Linear (LS)
					Bilinear (BS)
					Exponential (ES)
Four-point double-notched shear test	27.0	0.10	2.00	100.0	Linear (LS)
					Bilinear (BS)
					Exponential (ES)

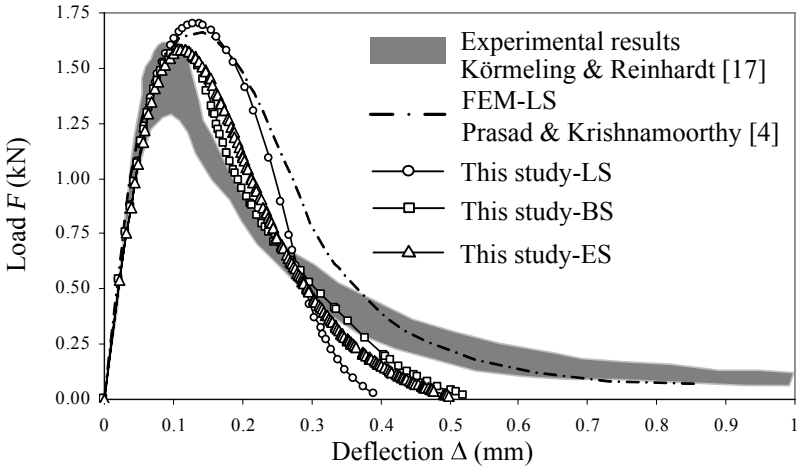

(a)

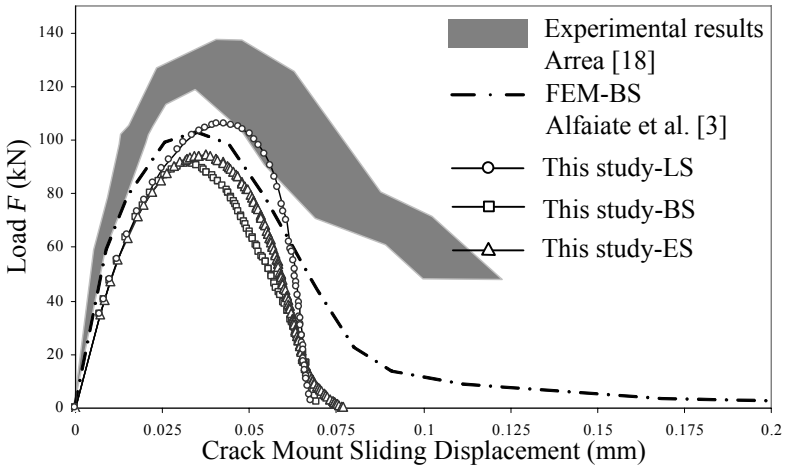

(b)

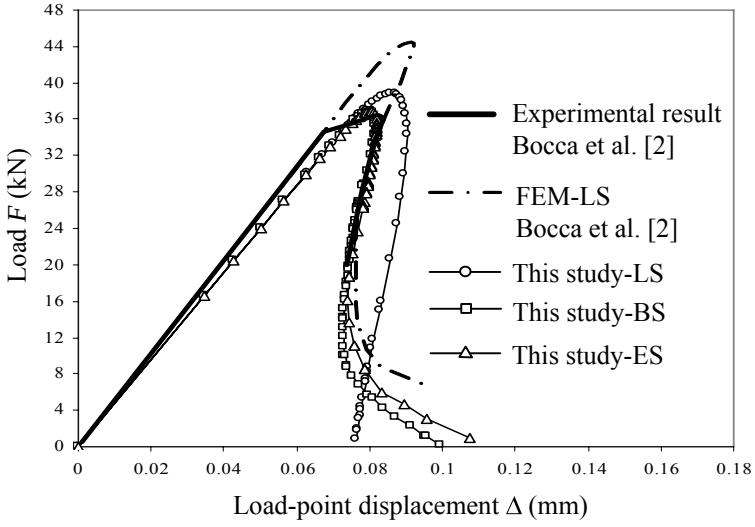

(c)

Fig. 6 Responses of the numerical examples

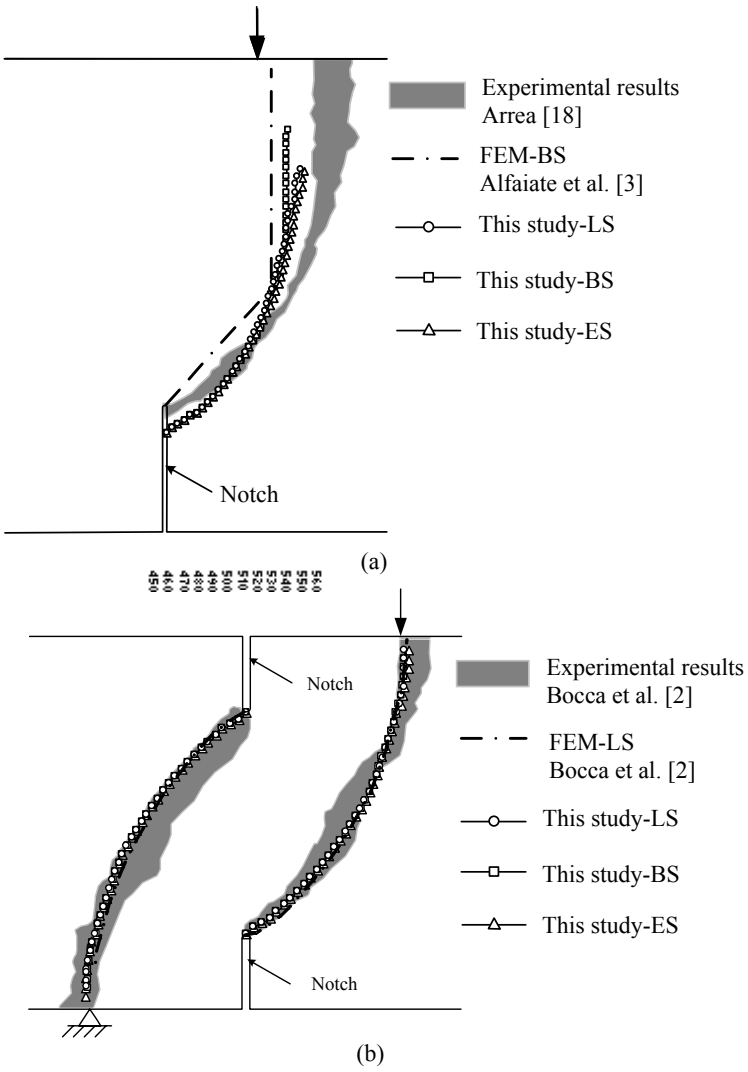

Fig. 7 Crack paths

5. Conclusions

In this paper, modeling of cohesive cracks in the Element-Free Galerkin (EFG) method is presented. Interface elements are used in the model to represent displacement discontinuities due to cracks. A curved crack is simply represented by connected straight-line interface elements. To simulate crack growth, the existing crack is lengthened in each incremental step by extending the crack line using an interface element. The interface elements permit the constitutive law of cohesive cracks to be considered directly and efficiently. The relative displacement increments between the two opposite surfaces of the interface elements are the crack displacement increments. The crack displacement increments are written in terms of the nodal displacement increments by using the EFG shape functions that employ the visibility criterion. To allow accurate analysis to be performed without the need of iteration, the stiffness equation of the domain is constructed by directly including a term related to the energy dissipation along the interface elements in the EFG weak form of the global system equation. If this energy term is not directly included in the derivation, the cohesive stresses on the crack surfaces will have to be treated as applied surface tractions. Subsequently, their magnitudes will have to be determined via iterations. The interface elements and the EFG method allow a crack to propagate without any constraint on its direction and without

remeshing. The analysis of example problems taken from the literature clearly shows the validity and efficiency of the proposed method. The results of the proposed method are found to be in good agreement with the FE and experimental results from the literature.

References

[1] A. Hillerborg, M. Modéer and P.-E. Petersson, "Analysis of Crack Formation and Crack Growth in Concrete by Means of Fracture Mechanics and Finite Elements", Cem. Concr. Res., Vol. 6, 1976, pp. 773-782.

[2] P. Bocca, A. Carpinteri and S. Valente, "Mixed Mode Fracture of Concrete", Int. Int. J. Solids Struct., Vol. 27, No. 9, 1991, pp. 1139-1153.

[3] J. Alfaiate, E.B. Pires and J.A.C. Martins, "A Finite Element Analysis of Non-Prescribed Crack Propagation in Concrete", Comput. Struct., Vol. 63, 1997, pp.17-26.

[4] M.V.K.V. Prasad and C.S. Krishnamoorthy, "Computational Model for Discrete Crack Growth in Plain and Reinforced Concrete", Comput. Methods Appl. Mech. Engrg., Vol. 191, 2002, pp. 2699-2725.

[5] J.C. Gálvez, J. Červenka, D.A. Cendón and V. Saouma, "A Discrete Crack Approach to Normal/Shear Cracking of Concrete", Cem. Concr. Res., Vol. 32, 2002, pp. 1567-1585.

[6] Z. Yang and J. Chen, "Full Automatic Modelling of Cohesive Discrete Crack Propagation in Concrete Beams Using Local Arc-Length Methods", Int. J. Solids Struct., Vol. 41, 2004, pp. 801-826.

[7] E.N. Dvorkin and A.P. Assanelli, "2D Finite Elements with Displacement Interpolated Embedded Localization Lines: The Analysis of Fracture in Frictional Materials", Comput. Methods Appl. Mech. Engrg., Vol. 90, 1991, pp. 829-844.

[8] G.N. Wells and L.J. Sluys, "Three-Dimensional Embedded Discontinuity Model for Brittle Fracture", Int. J. Solids Struct., Vol. 38, 2001, pp. 897-913.

[9] J. Alfaiate, G.N. Wells and L.J. Sluys, "On the Use of Embedded Discontinuity Elements with Crack Path Continuity for Mode-I and Mixed-Mode Fracture", Engrg. Fract. Mech., Vol. 69, 2002, pp. 661-686.

[10] T. Belytschko, Y.Y. Lu and L. Gu, "Element-Free Galerkin Methods", Int. J. Numer. Methods Engrg., Vol. 37, 1994, pp. 229-256.

[11] P. Lancaster and K. Salkauskas, "Surfaces Generated by Moving Least Squares Methods", Math. Comput., Vol. 37, No. 155, 1981, pp. 141-158.

[12] T. Belytschko, Y.Y. Lu, L. Gu and M. Tabbara, "Element-Free Galerkin Methods for Static and Dynamic Fracture", Int. J. Solids Struct., Vol. 32, No. 17-18, 1995, pp. 2547-2570.

[13] T. Belytschko and M. Tabbara, "Dynamic Fracture Using Element-Free Galerkin Methods", Int. J. Numer. Methods Engrg., Vol. 39, 1996, pp. 923-938.

[14] T. Belytschko and M. Fleming, "Smoothing, Enrichment and Contact in the Element-Free Galerkin Method", Comput. Struct., Vol. 71, 1999, pp. 173-195.

[15] B.N. Rao and S. Rahman, "An Efficient Meshless for Fracture Analysis of Crack", Comput. Mech., Vol. 26, 2000, pp. 398-408.

[16] T. Belytschko, D. Organ and C. Gerlach, "Element-Free Galerkin Methods for Dynamic Fracture in Concrete", Comput. Methods Appl. Mech. Engrg. Vol. 187, 2000, pp. 385-399.

[17] H.A. Körmeling and H.W. Reinhardt, Determination of the Fracture Energy of Normal Concrete and Epoxy Modified Concrete, Report 5-83-18, Delft University of Technology, Delft, 1983.

[18] M. Arrea, Mixed-Mode Crack Propagation in Mortar and Concrete, Master's Thesis, Cornell University, New York, 1982.